Chemical Physics Letters 455 (2008) 331–334

Contents lists available at ScienceDirect

Chemical Physics Letters

journal homepage: www.elsevier.com/locate/cplett

A new analysis of X-ray adsorption branching ratios: Use of Russell–Saunders coupling

Paul S. Bagus [a,*], Hajo Freund [b], Helmut Kuhlenbeck [b], Eugene S. Ilton [c]

[a] Department of Chemistry, University of North Texas, Denton, TX 76203-5070, USA
[b] Fritz-Haber-Institut der Max-Planck-Gesellschaft, Faradayweg 4-6, D-14195 Berlin, Germany
[c] Pacific Northwest National Laboratory, 902 Battelle Boulevard, P.O. Box 999, Richland, WA 99352, USA

ARTICLE INFO

Article history:
Received 8 October 2007
In final form 26 February 2008
Available online 2 March 2008

ABSTRACT

The intensities of X-ray absorption peaks at core-level edges are considered in terms of Russell–Saunders multiplets. The contributions of different multiplets to the relativistic wavefunctions of the excited states are determined and the absorption intensity related to the contributions of the dipole allowed multiplets. This is a powerful method because the selection rules for multiplets are stronger than for relativistic J levels. It is also shown that differences in the radial extent of the spin–orbit split core spinors modify the intensity given by these symmetry arguments. Applications are considered for cases involving different degrees of Russell–Saunders or *j*–*j* coupling.

The X-ray absorption near edge structure, XANES, of transition metal, TM, rare-earth, and actinide materials, typically have intense white lines at various absorption edges [1–6]. For a sufficiently large spin–orbit splitting, a doublet is observed corresponding to excitations from the $j = l + \frac{1}{2}$ and $j = l - \frac{1}{2}$ spin–orbit split core sub-shells. Thus, for example, the $L_{II,III}$ edge for transition metals will contain a peak, at lower photon energy, described as excitation from the $2p_{3/2}$ sub-shell into the 3d shell and a second peak, at higher photon energy, corresponding to excitation from the $2p_{1/2}$ sub-shell into the 3d shell [2]. For actinides, the $N_{IV,V}$ white line will be a doublet representing $4d_{5/2}$ and $4d_{3/2}$ excitations to the partly filled 5f shell. Of course, each of these spin–orbit split peaks may contain additional structure, often unresolved, of individual levels resulting from the intra-shell and inter-shell angular momentum coupling of the core and valence level open shells [4,6–10]. It is tempting to assign the relative intensities of the $l + \frac{1}{2}$ and $l - \frac{1}{2}$ peaks, or the branching ratios, to the statistical weights of the core levels [3]. For a transition metal $L_{II,III}$ edge, the relative intensities would be 2/3 and 1/3; for actinide $N_{IV,V}$ and $O_{IV,V}$ edges, they would be 3/5 and 2/5. However, it is well known that the angular momentum coupling strongly affects the branching ratios and the statistical values are appropriate only in special cases [9–11].

In the previous work of Thole and van der Laan [9], sum rules have been obtained that, for certain cases, allow the deviations of the branching ratios from the statistical values to be related to the spin–orbit splittings within the valence level. These sum rules have been derived using Clebsch–Gordon algebra and have not included the differences in the radial character of core orbitals for the $j = l - \frac{1}{2}$ and $j = l + \frac{1}{2}$ sub-shells [12]. They are based on atomic models used to describe condensed phase materials and they are applied for a range of occupations of the open valence level shell. In the present work, we also use atomic models. However, our objective is to relate transitions between Russell–Saunders, RS, multiplets [13], to transitions between the relativistic *J* levels that take account of spin–orbit coupling as well as of scalar relativistic effects. This approach offers physical insight into how different angular momentum couplings can affect the branching ratios since transitions between RS multiplets are easily understood from the dipole selection rules appropriate for XANES [14]. We base our work on four-component relativistic wavefunctions [15,16], WF's, that use spinors optimized separately for both the initial and the excited final states. These WF's use configuration interaction, CI, to describe the angular momentum coupling within and between the core and valence open shells and, thus, are able to properly treat the full range of intermediate coupling from RS ^{2S+1}L multiplets to pure *j*–*j* coupling [15].

Three cases are considered. The first is for the 2p or $L_{II,III}$ edge of V^{5+}, where as expected [4], the states are not pure $p_{3/2}$ or pure $p_{1/2}$ holes, denoted $p_{3/2}{}^{-1}$ and $p_{1/2}{}^{-1}$ respectively, but may involve significant mixing arising from the 2p–3d multiplet splitting. Here, we are also able to compare our predictions for the V^{5+} cation with our XANES measurements on V_2O_5 where the nominal V oxidation state is V^{5+}. The second is for the 4d or $N_{IV,V}$ edge of U^{6+}, where as expected from the large 4d spin–orbit splitting of ~40 eV, the excited states are nearly either pure $d_{5/2}{}^{-1}$ or $d_{3/2}{}^{-1}$ configurations. The third case is for the 5d or $O_{IV,V}$ edge of U^{6+} where we show that

* Corresponding author. Fax: +1 512 502 9760.
E-mail address: bagus@unt.edu (P.S. Bagus).

0009-2614/$ - see front matter © 2008 Elsevier B.V. All rights reserved.
doi:10.1016/j.cplett.2008.02.085

RS coupling dominates the character of the excited states and that this leads to an XANES 5d edge dominated by a single peak rather than by a doublet as for the other cases.

We have computed WF's for the initial and the core excited, final states with spinors optimized with Dirac–Fock calculations for the ground and excited configurations, respectively [15]. For the excited states, these optimized orbitals were used for a CI calculation with the core–hole distributed in all possible ways over the spinors of the core level and the electron placed in all possible ways over the spinors of the initially empty valence level. The dipole transition probabilities were computed rigorously between the initial and final state relativistic WF's taking full account of the non-orthogonality between the spinors of the initial and final states using a cofactor method [17,18]; see Ref. [8] for more details. The WF calculations were performed with the DIRAC program system [16]. For the wavefunctions of the non-relativistic RS multiplets, we used an artificially large speed of light raised to 10000 a.u. from its correct value of 137 a.u. We confirmed that this gave results equivalent to using a two component formalism where the spin–orbit coupling is not included in the Hamiltonian [15]. We then project the RS multiplets that could couple to $J = 1$ on the relativistic WF's in order to determine the extent of the RS composition of the dipole allowed, $J = 1$, core-excited levels. Here again, we took full account of the non-orthogonality between the relativistic spinors and the non-relativistic orbitals [8]. Since the only dipole allowed RS multiplet is $^1P_1$, The projection of this multiplet on each of the $J = 1$ levels should be a good guide to the relative intensity, I_{rel}, of the XANES excitation. For each edge, we also tabulated several properties which indicate the electronic character of the excited state.

In addition, we report $L_{II,III}$-edge XANES spectra for single crystal V_2O_5 recorded with light from the UE56 monochromator of the BESSY II synchrotron radiation facility in Berlin. The V_2O_5 crystals were obtained from the Paul-Drude Institut in Berlin where they were grown by zone melting [19]. They were fixed onto the sample holder of an UHV apparatus using electrically conductive silver glue. High quality (001) surfaces were obtained via in vacuo cleavage of the crystals using a sharp blade. This procedure is usually successful since V_2O_5 cleaves easily along the (001) plane. Since photon irradiation induces degradation of V_2O_5(001) a new surface was prepared from time to time. The data presented were measured in the total electron yield mode where the photocurrent emitted by the sample is measured with an electrometer as a function of the photon energy. Our use of total electron yield emphasizes the bulk XANES contribution over that from the V_2O_5 surface; more surface sensitive measurements can be made using partial electron yield [14]. However, even with partial electron yield, the contribution of the bulk to the XANES signal is still quite large; see, for example, Ref. [20].

For the L-edge of V^{5+}, the initial state is a closed shell, $J = 0$ and $^1S_0$, configuration and the dipole allowed, $J = 1$, excited states have the configuration $2p^53d^1$. This configuration couples to six RS multiplets, $^3F(J = 4,3,2)$, $^1F(J = 3)$, $^3D(J = 3,2,1)$, $^1D(J = 2)$, $^3P(J = 2,1,0)$, and $^1P(J = 1)$, where the possible J values are indicated in parenthesis after the ^{2S+1}L multiplet notation. For J levels, the dipole selection rules are $\Delta J = J(\text{initial}) - J(\text{final}) = 0, \pm 1$, where if $J(\text{initial}) = 0$ then $J(\text{final})$ must be one. The selection rules are stronger for RS multiplets because spin must be conserved so that $\Delta S = 0$ and $\Delta L = 0, \pm 1$. Thus, the only allowed final multiplet is $^1P_1$; however, this multiplet can mix into any of the three J levels. In terms of j–j coupling, the three configurations that can couple to $J = 1$ are: $2p_{1/2}{}^{-1}3d_{3/2}$, $2p_{3/2}{}^{-1}3d_{3/2}$, and $2p_{3/2}{}^{-1}3d_{5/2}$. The three relativistic $J = 1$ CI WF's are combinations of these j–j configurations. The E_{rel}, dipole I_{rel}, and the weights of the three j–j configurations are given in Table 1; the lowest $J = 1$ level is set to $E_{rel} = 0$ and the intensity of the second level is set to $I_{rel} = 1$; this normalization of I_{rel} is arbitrary. The first level has very little intensity, while the third is the most intense being roughly 2.5 times more intense than the second level. None of the levels is strongly dominated by a single j–j configuration although the highest level is 85% a $2p_{1/2}$ hole; clearly the excited states are not at the limit of j–j coupling. However, there is no basis for relating the weights of any of the j–j configurations to the I_{rel}.

In order to establish this relationship, we also give in Table 1 the projections of the Russell–Saunders multiplets, coupled to $J = 1$, on the relativistic CI WF's. These projections are normalized so that for a given $J = 1$ CI WF, the projections of $^1P_1$, $^3P_1$, and, $^3D_1$ sum to 1; i.e., they represent 100% of the relativistic WF. An independent check of the correctness of our projection is that, with this normalization, the sum of the projections of a single RS multiplet over the three $J = 1$ CI WF's, a sum over one of the 'Multiplet Character' columns in Table 1, is also one. Furthermore, the projection of these RS multiplets on the relativistic WF's with $J \neq 1$ is zero. For the dipole allowed ^1P multiplet, we also normalize the contributions of this multiplet to the different $J = 1$ levels to one for the second level; these values are given in parenthesis and permit a direct comparison with the I_{rel}. If the radial parts of the spinors for the different j values were identical, as assumed in Ref. [9] for the derivation of sum rules for branching ratios, then the relative contribution of the ^1P multiplet should be the same as the I_{rel}. We can see from Table 1 that this is nearly true for V; however, as we discuss below for the XANES of U, the approximation that the $j = l + \frac{1}{2}$ and $j = l - \frac{1}{2}$ spinors have the same radial character is less good for heavier atoms. While the lowest $J = 1$ level in the L-edge of V^{5+}, which receives almost no XANES intensity, is dominated by the ^3P multiplet, the two higher levels have significant mixing of ^3D and ^1P character. It is clear from the projections of the RS multiplets that WF's for the $2p \rightarrow 3d$ excited states of V^{5+} do not follow RS coupling with spin–orbit splitting of the ^{2S+1}L multiplets [13,21].

In Fig. 1, we present the XANES absorption intensities for light incident at 70° to the surface normal near the V L edge for V_2O_5. The XANES spectra taken with light incident at 0° are somewhat different from those shown in Fig. 1; however, until we take the V–O bonding and other ligand field effects into account, we cannot interpret these differences. These XANES studies are part of a broader effort [22] to identify the electronic structure of V_2O_5. The structures at ~519 eV and ~526 eV incident photon energy are associated with V $2p \rightarrow 3d$ excitations while other features at

Table 1
Properties of the three $J = 1$ levels of the $2p^53d^1$ configuration of V^{5+}

Level	E_{rel} (eV)	I_{rel}	Weight of j–j configurations			Multiplet character		
			$2p_{1/2}{}^{-1}3d_{3/2}{}^1$	$2p_{3/2}{}^{-1}3d_{3/2}{}^1$	$2p_{3/2}{}^{-1}3d_{5/2}{}^1$	^1P	^3P	^3D
1	0	0.02	0.02	0.74	0.24	0.5(0.02)	91.0	8.5
2	4.8	1	0.13	0.25	0.62	28.3(1)	4.4	69.3
3	11.9	2.44	0.85	0.00	0.15	71.2(2.52)	4.6	24.2

The relative energy, E_{rel} in eV, is set to zero for the first $J = 1$ level and the relative intensity, I_{rel}, is arbitrarily normalized to one for the second level. The weights of the j–j coupled $J = 1$ configurations and the projections, in %, of the Russell–Saunders multiplets on the relativistic CI WF's are also given; the ^1P multiplet projections normalized to one for the second level are given in parenthesis.

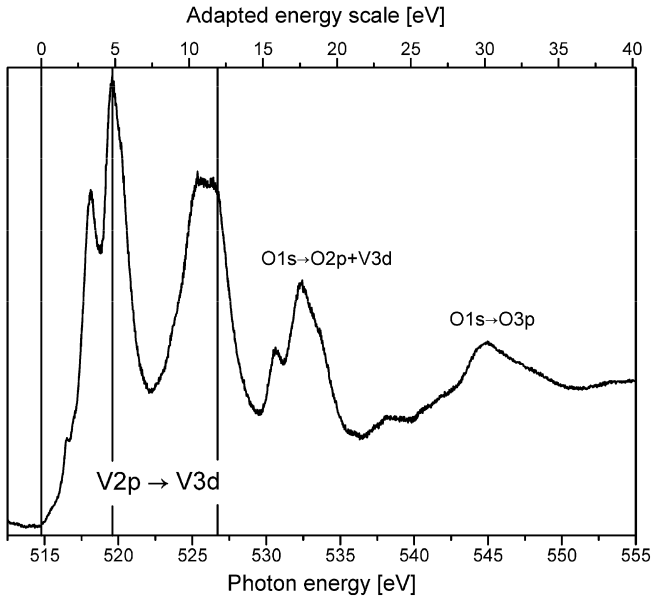

Fig. 1. XANES spectra of V_2O_5(0 0 1) for the $L_{II,III}$ edge of V, left hand area, and for the O 1s excitations, right hand area; the assignments are shown. The data were recorded in the total electron yield mode (see text) for a light incidence angle of $\Theta = 70°$ with respect to the surface normal. The shifted energy scale shown at the top was obtained by setting the energy of the first intense V2p feature to 4.8 eV which is the energy obtained by theory for level 2; the second vertical line is at 11.9 eV in the shifted energy scale, the position obtained by theory for Level 3 (see text and Table 1).

higher energy have their origin in O 1s excitations [22]. Clearly, the theoretical spectra in Table 1 do not reproduce the details of the experiment in Fig. 1. However, neglecting the very low I_{rel} first Level at $E_{rel} = 0$, the calculated 7.1 eV energy separation of Levels 2 and 3 is very close to the ~7 eV separation of the two $2p \rightarrow 3d$ peaks in Fig. 1. Furthermore, as predicted by our calculations, the intensities of these two XANES peaks are large. We believe that the additional features in the V_2O_5 XANES not in the atomic calculation and the different relative intensities of the measured and calculated spectra arise from ligand field effects, which are neglected in the atomic model. However, our simple atomic model allows us to understand that there are two intense peaks based on the contribution of the dipole allowed ^1P multiplet to the WF's for the intermediate coupling for the $2p^53d^1$ configuration. Of course, this atomic contribution is modified by the ligand field splitting of the d levels in V_2O_5. As the coupling changes to being either more nearly *j–j* or RS, the intensities and energy spacings of the XANES peaks will change.

A similar analysis is presented for the $N_{IV,V}$ edge of closed shell U^{6+} where the excited states have the configuration $4d^95f^1$; and where the dipole allowed excitations from the $^1S_0$ ground state are to $J = 1$ excited states. For $4d^95f^1$, there are three RS multiplets, ^3D, ^3P, and ^1P, that can couple to $J = 1$ levels but only the $^1P_1$ is dipole allowed for XANES excitation from the $^1S_0$ initial state. The same properties given for the V^{5+} L-edge in Table 1 are given for the U^{6+} N-edge in Table 2. As for the V^{5+} L-edge, the first $J = 1$ level for the N-edge of U^{6+} has very little intensity; however, now the second level at $E_{rel} = 2.3$ eV has the largest intensity while the third level at $E_{rel} = 44.4$ eV has only 55% of this intensity. From the weights of the *j–j* configurations, it is clear that the WF's for these *J* levels have nearly pure *j–j* coupling with almost no mixing of configurations that have a $4d_{3/2}$-hole with those that have a $4d_{5/2}$-hole. There is, however, some mixing of the $5f_{5/2}$ and $5f_{7/2}$ occupations that is driven by exchange-like electrostatic integrals between the 4d and 5f spinors [13,21,23]. These integrals are expected to be small because of the very different spatial extents of the 4d and 5f orbitals [12]. Since the coupling is nearly pure *j–j* coupling, we find that the WF's for all the levels contain substantial mixings of the different RS multiplets.

For the U^{+6} N-edge, the projection of the RS ^1P multiplet on the relativistic WF's for the $J = 1$ levels also provides a useful guide to the I_{rel}; see Table 2. However, the projection of the ^1P multiplet predicts a relative intensity for the third $J = 1$ level that is ~30% larger than the rigorously calculated I_{rel}. It is easy to understand why the values of I_{rel} are different from the intensities estimated from the projections of the ^1P multiplet on the $J = 1$ WF's for the N-edge of U^{+6} if we consider the differences in the radial character of the $j = l + \frac{1}{2}$ and $j = l - \frac{1}{2}$ spinors. For convenience of calculation [16], we use $\langle r^2 \rangle$ as a measure of the sizes or radial extents of the $j = l \pm 1/2$ spinors of the edge that is studied, 2p for V^{5+} and 4d for U^{6+} where the $\langle r^2 \rangle$ are computed for the variationally optimized spinors of the initial state. The spatial extent of the $J = l + \frac{1}{2}$ spinor is expected to be larger than that of $j = l - \frac{1}{2}$ [12,24]; of course, the magnitude of the difference depends on the nuclear charge and the shell.

The projections of the RS multiplets are determined by the symmetry of the WF's and do not use the one-electron dipole transition integrals. The effect of this neglect is to overestimate the intensity of the higher energy excited state dominated by excitation of the $j = l - \frac{1}{2}$ spinor since the transition matrix elements for this spinor are smaller than for $j = l + \frac{1}{2}$. On the other hand, our calculation of I_{rel} rigorously and explicitly includes the dependence of the electric dipole transition integrals on the radial character of the spinors. From Table 1, the relative intensity of the highest energy excitation for V^{5+} calculated with I_{rel} is 2.44, only slightly smaller than the estimate of 2.52 obtained from the projection of the $^1P_1$ RS multiplet. The small decrease with the more accurate I_{rel} comes from the fact that $\langle r^2 \rangle_{2p1/2}$ is less than 2% smaller than $\langle r^2 \rangle_{2p3/2}$. However, see above, the accurate I_{rel} for the U^{6+} N-edge is 30% smaller than estimated from the projection because the $\langle r^2 \rangle$ for $4d_{3/2}$ is over 6% smaller than for $4d_{5/2}$. Thus, taking direct and accurate account of the one-electron dipole transition integrals is necessary for U.

We note that when the I_{rel} are cast as branching rations with $B = I(5/2)/[I(5/2)+I(3/2)]$ then the difference becomes smaller; the rigorous *B* obtained using the I_{rel} is 0.64 while the approximate *B* obtained from the projection is 0.58. Our value of $B = 0.58$ obtained with projection should be the same as the value obtained from the sum rule analysis of van der Laan et al. [4], $B = 0.59$, since in neither case are the dipole integrals between spinors explicitly taken in account. Clearly, neglect of the dipole integrals, either in sum rules [4] or in our projection introduces a 10% error in the branching ratio for U and this could become even larger for heavier actinides.

Table 2
Properties of the three $J = 1$ levels of the $4d^95f^1$ configuration of U^{6+}; see the caption to Table 1

Level	E_{rel} (eV)	I_{rel}	Weight of *j–j* configurations			Multiplet character		
			$4d_{3/2}{}^{-1}5f_{5/2}{}^{1}$	$4d_{5/2}{}^{-1}5f_{5/2}{}^{1}$	$4d_{5/2}{}^{-1}5f_{7/2}{}^{1}$	^1P	^3P	^3D
1	0	0.01	0.00	0.90	0.10	0.5(0.01)	73.2	26.4
2	2.3	1	0.00	0.10	0.90	57.7(1)	8.1	34.1
3	44.4	0.55	1.00	0.00	0.00	41.7(0.72)	18.5	39.7

Table 3
Properties of the three $J = 1$ levels of the $5d^95f^1$ configuration of U^{6+}; see the caption to Table 1

Level	E_{rel} (eV)	I_{rel}	Weight of j–j configurations			Multiplet character		
			$5d_{3/2}{}^{-1}5f_{5/2}{}^{1}$	$5d_{5/2}{}^{-1}5f_{5/2}{}^{1}$	$5d_{5/2}{}^{-1}5f_{7/2}{}^{1}$	^1P	^3P	^3D
1	0	0.00	0.03	0.83	0.14	0.1(0.00)	86.5	13.5
2	6.9	0.03	0.42	0.15	0.43	2.2(0.02)	12.9	84.8
3	31.2	1	0.55	0.02	0.43	97.8(1)	0.6	1.7

Finally, we turn to the $O_{IV,V}$ edge of U^{6+} where the excited configuration is $5d^95f^1$. This analysis very closely parallels that for the $N_{IV,V}$ edge although the results, presented in Table 3, are quite different. In Table 3, the format is slightly changed and I_{rel} for the O-edge of U is normalized to one for the intense transition to the third excited $J = 1$ level at $E_{rel} = 31$ eV rather than to the second J level as in Table 2; the normalized ^1P projections are also scaled to one for the third level. The only transition that carries significant intensity is to the third level and a single intense feature with a weak satellite, at lower excitation energy, from the second level should be observed, in strong contrast to the doublet predicted for the N-edge. The mixing of the j–j configurations is even greater for the O-edge excitation of U^{6+} than for the L-edge excitation of V^{5+}; this is hardly surprising since the 5d spin–orbit splitting is small compared to the splitting of the Russell–Saunders multiplets. We estimate a 5d spin–orbit splitting of 8.7 eV from the Dirac–Fock eigenvalues of the $5d_{3/2}$ and $5d_{5/2}$ spinors for the ground state of U^{6+}. We estimate the multiplet splitting from the energy spread in our non-relativistic calculations on the $5d^95f^1$ configuration where the lowest energy multiplet is ^3P and the highest energy multiplet is ^1P; the ^3P-^1P energy separation of 30.2 eV is taken as the multiplet splitting. Thus, while the multiplet splitting should be more important than the 5d spin–orbit splitting, the levels may be significantly perturbed from pure RS multiplets. We can see this for the first two levels where the dominant RS multiplet is only 85% of the total WF. The XANES spectra for the $O_{IV,V}$ edge of UO_3, with a nominal oxidation state of U(VI), have been measured [25] and show a strong main peak with a very weak satellite at lower energy; this is fully consistent with our theoretical analysis.

We have shown that examining the contribution of dipole allowed X-ray adsorption multiplets to the relativistic atomic WF's for J levels of a closed shell initial state provides insight into the origin of the energies and intensities of XANES excitations. We stress that we have neglected the changes caused by the environment in condensed phases, especially ligand field effects in oxides and other ionic crystals. Because we have used atomic models, we cannot explain the fine details of the XANES edges, including energy splittings and intensity changes that arise from condensed phase effects. However, our analysis in terms of RS multiplets has made it possible to have a qualitative understanding of the number and relative intensities of the main peaks that are observed at a particular XANES edge. Furthermore, we have shown that neglect of the difference of radial matrix elements for spin–orbit split levels, as in sum rules [4] and projections introduces a modest uncertainty in the branching ratio that could become larger for heavier actinides and for the edges of deeper core levels.

We have examined three cases: (1) the $N_{IV,V}$-edge of U^{6+} with $4d \rightarrow 5f$, where j–j coupling dominates, especially for the core level; (2) the $O_{IV,V}$-edge of U^{6+} with $5d \rightarrow 5f$ where Russell–Saunders coupling dominates; and, (3) the $L_{II,III}$-edge of V^{5+} with $2p \rightarrow 3d$ where the coupling is strongly mixed. While we have considered the case of a closed shell initial state where only a single RS excited state multiplet is dipole allowed, our logic of decomposing initial and excited state relativistic WF's into the contributions from various multiplets can be applied to more complex cases.

This research was supported, in part, by the Geosciences Research Program, Office of Basic Energy Sciences, US Department of Energy (DOE). A portion of the research was performed at the W.R. Wiley Environmental Molecular Sciences Laboratory, a national scientific user facility sponsored by the US DOE. We acknowledge partial computer support from the National Center for Supercomputing Applications, Urbana-Champaign, Illinois.

References

[1] J. Stohr, D.A. Outka, K. Baberschke, et al., Phys. Rev. B 36 (1987) 2976.
[2] F.M.F. de Groot, J. Electron Spectrosc. Relat. Phenom. 67 (1994) 529.
[3] K.T. Moore, M.A. Wall, A.J. Schwartz, et al., Phys. Rev. Lett. 90 (2003) 196404.
[4] G. van der Laan, K.T. Moore, J.G. Tobin, et al., Phys. Rev. Lett. 93 (2004) 097401.
[5] H. Ogasawara, A. Kotani, B.T. Thole, Phys. Rev. B 44 (1991) 2169.
[6] A. Kotani, H. Ogasawara, Physica B 186–188 (1993) 16.
[7] P.S. Bagus, R. Broer, W.A. de Jong, et al., Phys. Rev. Lett. 84 (2000) 2259.
[8] P.S. Bagus, E.S. Ilton, Phys. Rev. B 73 (2006) 155110.
[9] B.T. Thole, G. van der Laan, Phys. Rev. A 38 (1988) 1943.
[10] B.T. Thole, G. van der Laan, Phys. Rev. B 38 (1988) 3158.
[11] G. van der Laan, B.T. Thole, Phys. Rev. Lett. 60 (1988) 1977.
[12] J.P. Desclaux, At. Data Nucl. Data Tables 12 (1974) 311.
[13] J.C. Slater, Quantum Theory of Atomic Structure, vols. I and II, McGraw-Hill, New York, 1960.
[14] J. Stöhr, NEXAFS Spectroscopy, Springer-Verlag, Berlin, 1992.
[15] L. Visscher, O. Visser, P.J.C. Aerts, et al., Comput. Phys. Commun. 81 (1994) 120.
[16] T. Saue, V. Bakken, T. Enevoldsen, et al., Dirac, a relativistic ab initio electronic structure program, Release 3.2, 2000.
[17] F. Prosser, S. Hagstrom, Int. J. Quantum Chem. 2 (1968) 89.
[18] F. Prosser, S. Hagstrom, J. Chem. Phys. 48 (1968) 4807.
[19] F. Jachmann, C. Hucho, Solid State Commun. 135 (2005) 440.
[20] A.C. Dupuis, M. Abu Haija, B. Richter, et al., Surf. Sci. 539 (2003) 99.
[21] E.U. Condon, G.H. Shortly, The Theory of Atomic Spectra, Cambridge University Press, Cambridge, 1951.
[22] C. Kolczewski, K. Hermann, J. Chem. Phys. 118 (2003) 7599.
[23] J.S. Griffith, The Theory of Transition-Metal Ions, Cambridge Press, Cambridge, 1971.
[24] H.A. Bethe, E.W. Salpeter, Quantum Mechanics of One- and Two-Electron Atoms, Academic Press, 1957.
[25] G. Kalkowski, G. Kaindl, W.D. Brewer, et al., Phys. Rev. B 35 (1987) 2667.